Mechatronics 24 (2014) 906–913

Contents lists available at ScienceDirect

Mechatronics

journal homepage: www.elsevier.com/locate/mechatronics

Coupling Bond Graph and Energetic Macroscopic Representation for Electric Vehicle Simulation

L.I. Silva [a,*], A. Bouscayrol [b], C.H. De Angelo [a], B. Lemaire-Semail [b]

[a] Grupo de Electrónica Aplicada (GEA), Universidad Nac. de Río Cuarto, Argentina
[b] Lab. d'Electrotechnique et d'Electronique de Puissance (L2EP), Univ. Lille1, France

ARTICLE INFO

Article history:
Received 27 February 2013
Revised 22 October 2013
Accepted 23 December 2013
Available online 23 January 2014

Keywords:
Energetic Macroscopic Representation
Bond Graph
Electric Vehicle Simulation

ABSTRACT

This paper deals with the analysis and simulation of an electric vehicle, coupling functional and structural approaches in the same simulation environment. The Bond Graph model, the structural approach, is first deduced from the physical system, which in turn produces a direct correspondence between the system and its model. The control structure is then easily deduced from the Energetic Macroscopic Representation, the functional approach, of the vehicle using a systematic procedure. Simulation results are provided in order to analyze the performance of the closed-loop system.

1. Introduction

Electric Vehicles (EVs) and Hybrid Electric Vehicles (HEVs) have been investigated as an alternative solution to mitigate the problems of fossil fuel depletion and pollutant emissions [1]. Simulation is a key issue in the design stage given that it allows the evaluation of different vehicle concepts and control configurations. These benefits can be exploited rapidly, inexpensively and without implementing a prototype [2]. Two different descriptions are generally used: a structural description and a functional one [3].

A structural description organizes the model based on the topology of the system. Structural software such as PSIM® enables us to easily build the system for analysis and design [4]. The Bond Graph (BG) method [5] is a graphical structural description suited to model large scale physical systems independently of their nature [6]. For this reason BG is useful for modeling multi-domain systems in general and the electrical/mechanical/thermal nature of an EV [7] or HEV [8] in particular.

A functional description focuses on the functions of the system and is oriented toward control design. Functional software, such as those presented in [9–11], are useful for control design and assessment. The classical block diagrams approach is generally used but new graphical tools have been developed for the description of complex systems [3]. Energetic Macroscopic Representation (EMR) is a graphical functional description that allows us to systematically find the control schemes for complex energetic systems [12,13].

Both descriptions have been used to study EVs and HEVs in recent literature. On the one hand, it is possible to use functional representations for simulating different controls applied to HEVs [14,15]. On the other hand, in [16,17] novel fault detection strategies based on a complete structural representation of the vehicle are proposed. The first coupling between a structural and a functional approach was proposed in [18] where a power system is simulated using PSIM®. The system is simulated using a structural component library and the control is designed using EMR.

The objective of this research is to couple, in the same simulation environment, BG and EMR for the description of an EV and its control. This proposal allows us to exploit the advantages of each approach applied to the analysis and control of a complete EV traction system.

Section 2 presents the proposed model of the studied EV. In Section 3 the control scheme of the vehicle is obtained based on its EMR. Simulation results presented in Section 4 illustrate the performance of the designed control.

2. Modeling and representation of the vehicle

The model of the studied EV is shown in Fig. 1(a). It is powered by a battery which supplies a permanent magnet DC machine through a chopper. The DC machine is connected to a gearbox which turns the shafts of the frontal wheels through the mechanical differential. The representation of the EV model using BG (see Fig. 1(b)) presents a direct correspondence with the physical structure of the system. In order to depict the variables of interest, effort sensors were added in the BG. From the model it is also possible to

* Corresponding author. Tel.: +54 03584676255.
E-mail addresses: lsilva@ing.unrc.edu.ar, lsilva@ieee.org (L.I. Silva).

0957-4158/$ - see front matter © 2014 Elsevier Ltd. All rights reserved.
http://dx.doi.org/10.1016/j.mechatronics.2013.12.010

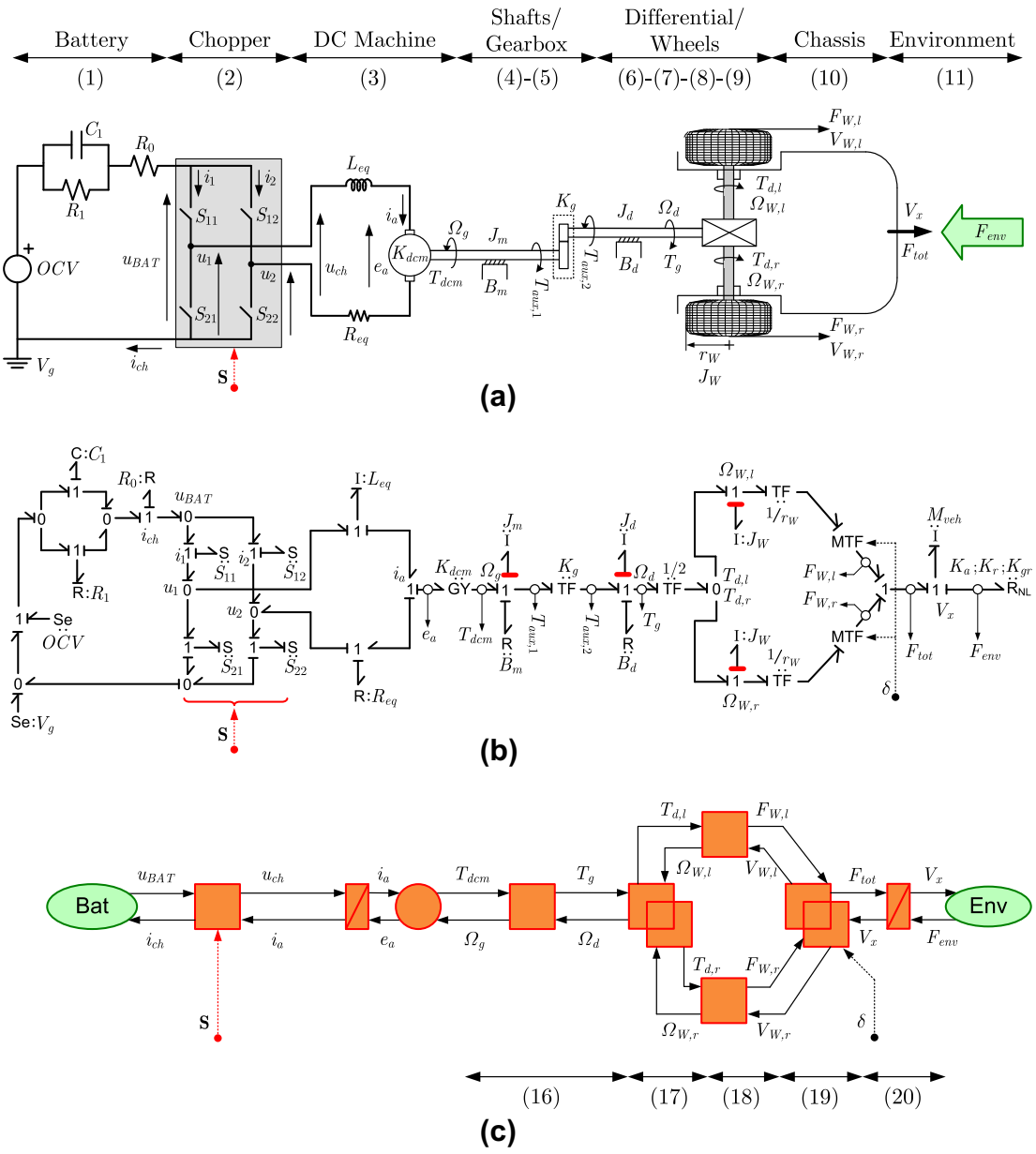

Fig. 1. (a) Electric vehicle scheme, (b) BG representation, and (c) Energetic Macroscopic Representation. *Note:* The numbers in brackets correspond to equations throughout the paper.

derive its EMR, as shown in Fig. 1(c), thus giving a synthetic and functional point of view of the system.

2.1. Proposed model

The battery imposes the voltage (u_{BAT}) as a function of the State Of Charge (SOC) of the battery [19]. In addition, the SOC is obtained based on the current (i_{ch}) demanded by the chopper and, alternatively, the temperature of the electrolyte (θ) as follows:

$$\begin{aligned} u_{BAT} &= f(SOC) \\ SOC &= f(i_{ch};\theta) \end{aligned} \tag{1}$$

As a first approach, the chopper model considers ideal switches without losses. The signal input **S** contains four boolean variables which determine if the switch is on or off ($S_{ij}=1$ and $S_{ij}=0$, respectively). Moreover, within the same leg, one signal is always the complement of the other; i.e. when a switch is open the other is closed and vice versa. Voltages and currents are related as shown:

$$\begin{aligned} u_{ch} &= u_1 - u_2 = (S_{11} - S_{12})\, u_{BAT} \\ i_{ch} &= i_1 + i_2 = (S_{11} - S_{12})\, i_a \end{aligned} \tag{2}$$

where $S_{ij} \in \{0,1\}$; u_{ch} and i_a are respectively the output voltage of the chopper and the armature current of the DC machine.

The dynamics of the DC machine is given by:

$$\begin{aligned} u_{ch} - e_a &= R_{eq} i_a + L_{eq} \frac{d}{dt}(i_a) \\ e_a &= K_{dcm} \Omega_g \\ T_{dcm} &= K_{dcm} i_a \end{aligned} \tag{3}$$

where L_{eq} and R_{eq} are the inductance and resistance of the windings, respectively. The electromechanical conversion is assumed ideal (without losses) where the relation between the electrical and mechanical variables is given by the constant of the motor (K_{dcm}). This parameter relates the angular speed of the motor shaft (Ω_g) with the electromotive force (e_a), as well as the produced torque (T_{dcm}) with the armature current.

Assuming that friction the phenomenon in the motor shaft is due to viscous friction, the dynamics are given by:

$$J_m \frac{d}{dt}(\Omega_g) = T_{dcm} - B_m \Omega_g - T_{aux,1} \tag{4}$$

where J_m and B_m are the moment of inertia and friction coefficient of the shaft, respectively. Load torque at the end of the shaft is designated as $T_{aux,1}$.

The gearbox is assumed ideal (i.e. power losses, mechanical backlash, hysteresis and elasticity effects are neglected). It has a fixed ratio (K_g) which relates Ω_g to the angular speed of the differential shaft (Ω_d) and the torques on each side of the gearbox ($T_{aux,1}$ and $T_{aux,2}$), as follows:

$$\begin{aligned} T_{aux,2} &= K_g T_{aux,1} \\ \Omega_g &= K_g \Omega_d \end{aligned} \tag{5}$$

Considering only viscous friction in the shaft of the differential, the dynamics can be expressed as:

$$J_d \frac{d}{dt}(\Omega_d) = T_{aux,2} - B_d \Omega_d - T_g \tag{6}$$

where J_d and B_d are the moment of inertia and friction coefficient of the differential shaft, respectively. The net torque generated at the end of the complete gearbox is defined as T_g.

The mechanical differential allows different angular velocities on each wheel (Ω_W) while the same torque is applied (T_d). Their relations are expressed as follows:

$$\begin{aligned} T_{d,l} &= T_{d,r} = \frac{1}{2}(T_g) \\ \Omega_d &= \frac{1}{2}(\Omega_{W,l} + \Omega_{W,r}) \end{aligned} \tag{7}$$

The model of the wheels may include complex phenomena such as mechanical friction and tire/road interaction [20]. For the purpose of this study these phenomena are neglected and the behavior is given by:

$$J_W \frac{d}{dt}(\Omega_{W,i}) = T_{d,i} - T_{W,i} \rightarrow i \in \{l, r\} \tag{8}$$

where r_W is the radius and J_W is the moment of inertia. The force at the patch contact (F_W) is related to the tangential velocity (V_W) as follows:

$$V_{W,i} = \Omega_{W,i}\, r_W \; T_{W,i} = F_{W,i}\, r_W \rightarrow i \in \{l, r\} \tag{9}$$

The chassis model includes lateral motion based on the geometric model [21] which relates V_W to the vehicle's velocity (V_x), steering angle (δ), distance between left and right wheels (d) and the distance between rear and front wheels (l). It also includes the longitudinal dynamics by computing V_x based on the total force (F_{tot}), the force produced by the environment (F_{env}) and the mass of the vehicle (M_{veh}). These relations are given by:

$$\begin{aligned} V_{W,l} &= \left(1 - \frac{\mathrm{tg}(\delta)}{l}\frac{d}{2}\right) V_x \\ V_{W,r} &= \left(1 + \frac{\mathrm{tg}(\delta)}{l}\frac{d}{2}\right) V_x \\ F_{tot} &= F_{W,l} + F_{W,r} \\ F_{tot} - F_{env} &= M_{veh}\frac{d}{dt}(V_x) \end{aligned} \tag{10}$$

Finally the interaction with the environment is considered. The force F_{env} is composed of the aerodynamic dragging force (F_{aero}), the rolling resistance (F_{roll}) and the component of the vehicle's weight when it meets a slope (F_{grade}). This is expressed as:

$$\begin{aligned} F_{env} &= F_{aero} + F_{roll} + F_{grade} \\ F_{aero} &= K_a V_x^2 \rightarrow K_a = \frac{1}{2}\rho_{air} A_f C_x \\ F_{roll} &= K_r M_{veh} g \\ F_{grade} &= K_{gr} M_{veh} g \rightarrow K_{gr} = \sin(\varphi) \end{aligned} \tag{11}$$

where ρ_{air}, A_f and C_x are the air density, the frontal area of the vehicle and the aerodynamic coefficient, respectively. The rest of the required parameters are the rolling resistance coefficient (K_r) and the angle of the slope (φ).

2.2. Bond Graph representation

This formalism facilitates the construction of models that represent the dynamics of multi-domain systems. The BG contains dissipative, accumulative and conversion elements and junctions. The elements are interconnected by bonds which carry the exchange variables (general flow and effort) and allow an easy visualization of the physical system topology and power flow. For more details regarding the BG elements, refer to Appendix A.

The model of the battery given in Fig. 1(a) can be extended to represent both Lead–Acid and Li-Ion batteries, as proposed in [22]. The new model includes a parasitic branch (R_p), a new internal resistance (R_2) and a capacitor (C_e) in series with the voltage source (see Fig. 2(a)). Now the output current of the battery (current demanded by the chopper i_{ch}) is computed as the current through the main branch (i_m) minus the parasitic current (i_p). Using this model, it is possible to study the complete EV energy performance under different driving conditions [23].

The electric elements involved depend on the temperature of the electrolyte (θ), the State Of Charge (SOC) and the Depth Of Charge (DOC) of the battery which are computed as follows:

$$\begin{aligned} SOC &= 1 - \frac{Q_e}{C(0;\theta)} \rightarrow C(0;\theta) = C_0(1 - \theta/\theta_f)^{\epsilon} \\ DOC &= 1 - \frac{Q_e}{C(i_m;\theta)} \rightarrow C(i_m;\theta) = C_0 \frac{K_c(1 - \theta/\theta_f)^{\epsilon}}{1 + (K_c - 1)(i_m/I^*)^{\delta}} \end{aligned} \tag{12}$$

where $Q_e = \int -i_m dt$ and the initial condition is assumed fully charged. The parameters of the electric elements involved can now be computed as follows:

$$\begin{aligned} C_e &= C_0 \frac{K_c(1 - \theta/\theta_f)^{\epsilon}}{K_e \theta}; \quad R_0 = R_{00}[1 + A_0(1 - SOC)] \\ R_1 &= -R_{10}\ln(DOC); \quad C_1 = \tau_1/R_1 \\ R_2 &= R_{20}\frac{\exp[A_{21}(1 - SOC)]}{1 + \exp[A_{22}(i_m/I^*)]}; \quad R_p = \frac{1}{G_{p0}\exp[u_p/u_{p0} + A_p(1 - \theta/\theta_f)]} \end{aligned} \tag{13}$$

The proposed model for the battery is assumed isothermal; θ thus becomes a constant parameter. Moreover, the electrochemical dynamics are not apparent, given that the model consists of an electrical network that interpolates the battery behavior, as seen from the terminals. Nevertheless the BG representation can be easily extended in order to include thermal dynamics and can be modify in order to represent the electrochemical dynamics within the battery. For details about BG representations, including thermal and electrochemical dynamics, refer to [24].

Fig. 2(a) also depicts a more detailed model of the chopper. The model of the chopper contains four switches composed of a semiconductor device with an antiparallel diode. This element can be represented as an ideal switch with its ohmic resistance R_{on} and another resistance in parallel R_{off} (see the dotted square in Fig. 2(a)).

The BG representation of the new battery-chopper model is obtained in a straightforward manner, as shown in Fig. 2(b). The

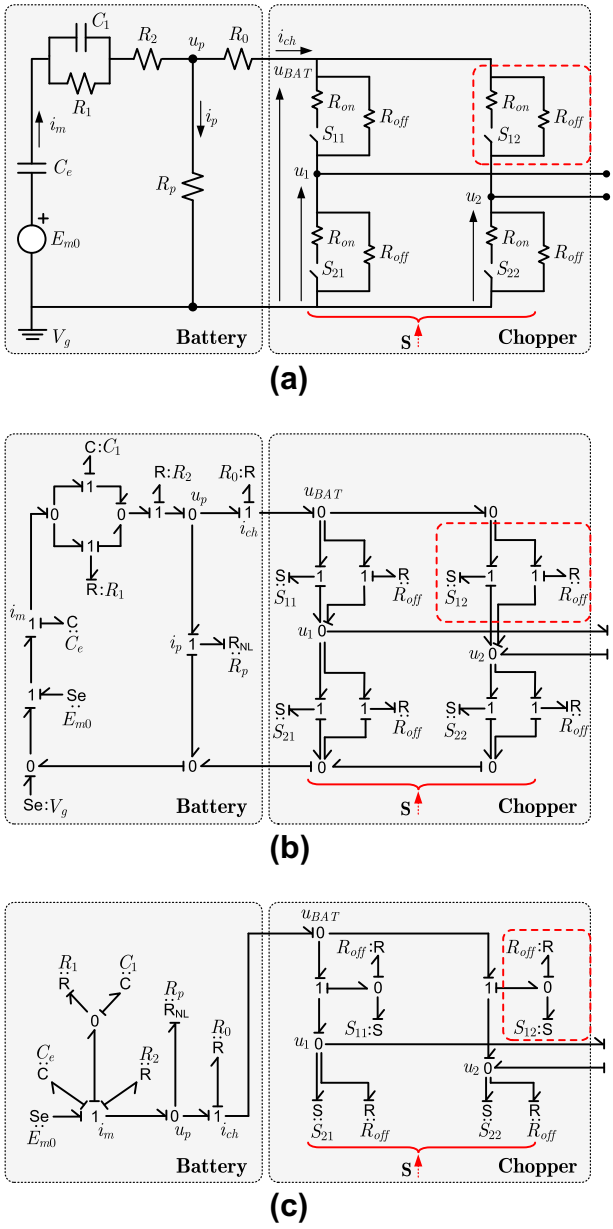

Fig. 2. (a) Detailed model of battery and chopper, (b) complete BG representation, and (c) simplified BG with thermal dynamics.

BG model of each switch is based on [25,26] (see dotted square of Fig. 2(b)). Each ideal switching element **S** receives a boolean signal S_{ij} and computes, with fixed causality, the flow (f_{ij}) as a function of the effort (e_{ij}), as follows:

$$f_{ij} = S_{ij}\frac{1}{R_{on}}e_{ij} \tag{14}$$

Assuming $V_g = 0$, the BG representation is simplified. This simplified version is depicted in Fig. 2(c).

The rest of the vehicle representation in BG includes the DC machine, the mechanical system and the environment, as proposed in Fig. 1(b). The complete BG representation of the physical system is proposed in the upper part of Fig. 4. It can be seen that some accumulative elements are written in derivative causality even though integral causality is preferred (derivative causality is noted using an orange bold bar). In order to avoid derivative causality, two solutions could be put in place:

- Modify the original hypotheses and include elasticity in the shafts and wheels.
- Merge the accumulative elements with derivative causality into an accumulative element with integral causality. This generates a new equivalent element [27].

The advantage of representing our model with derivative causalities, as shown in Fig. 1(b), is that all accumulative elements are included and placed according to the topology and the original hypotheses are maintained. This characteristic enables the possibility of including faults in these components in order analyze the impact on the overall behavior.

A contribution of this proposal is that the mathematical model governing the dynamics of the entire system can be obtained systematically from the BG representation [27]. Due to the simplicity of our case of study, Eqs. (1)–(11) are obtained using first principles, but for large scale physical systems this procedure becomes crucial.

2.3. Energetic Macroscopic Representation

EMR makes apparent the power interchange between components and sub-systems. It is composed of connected elements which highlights the energy properties of the system (e.g. energy source, accumulation, conversion, and distribution). It gives an overall idea of the energy distribution within the system. An additional advantageous feature of EMR is that it allows us to determine in a systematic way an inversion-based control scheme. Further details about the elements used in EMR are given in Appendix A.

The EMR of the vehicle is depicted in Fig. 1(c). It is composed of connected elements that highlight the energy properties of the EV. Connections are based on the action–reaction principle.

Its construction can be easily achieved using the set of Eqs. (1)–(11) which corresponds to each sub-system. In this case, unlike the BG representation, all accumulative elements must be in integral causality. As an example, in Fig. 1(c), it can be seen that the accumulative element representing the inductance of the windings determines the armature current (i_a) based on the inductance voltage (V_L), as follows:

$$\begin{aligned} i_a(t) &= i_a(t_0) + \frac{1}{L_{eq}}\int_{t_0}^{t} V_L(\tau)\, d\tau \\ V_L &= u_{ch} - e_a - R_{eq} i_a \end{aligned} \tag{15}$$

This expression is the integral version of the first line in (3).

In order to maintain the integral causality, some additional analysis is needed when two different accumulative elements try to impose the same state variable. This conflict of association is solved using the permutation and merging rules [28]. First the accumulative elements in conflict are "moved" together (permutation) and then an equivalent accumulative element (merging) is generated. In the final EMR the accumulative elements representing the inertia of the machine shaft (J_m), the differential shaft (J_d) and the inertia of the wheels (J_W) are incorporated in the equivalent accumulative element of the chassis.

The new set of equations of the resulting EMR depicted in Fig. 1(c) are the following:

$$\begin{aligned} T_g &= K_g T_{dcm} \\ \Omega_g &= K_g \Omega_d \end{aligned} \tag{16}$$

$$\begin{aligned} T_{d,l} &= T_{d,r} = \frac{1}{2}(T_g) \\ \Omega_d &= \frac{1}{2}(\Omega_{W,l} + \Omega_{W,r}) \end{aligned} \tag{17}$$

$$F_{W,i} = \frac{T_{d,i}}{r_W} \rightarrow i \in \{l, r\}$$
$$\Omega_{W,i} = \frac{V_{W,i}}{r_W} \rightarrow i \in \{l, r\} \tag{18}$$

$$V_{W,l} = \left(1 - \frac{\mathrm{tg}(\delta)}{l}\frac{T}{2}\right)V_x$$
$$V_{W,r} = \left(1 + \frac{\mathrm{tg}(\delta)}{l}\frac{T}{2}\right)V_x \tag{19}$$
$$F_{tot} = F_{W,l} + F_{W,r}$$

$$V_x(t) = V_x(t_0) + \frac{1}{M_{eq}}\int_{t_0}^{t}\sum F(\tau)\, d\tau$$
$$\sum F = F_{tot} - F_{env} - B_{eq}V_x$$
$$M_{eq} = M_{veh} + \frac{1}{r_W^2}\left(2J_W + J_d + \frac{1}{K_g^2}J_m\right) \tag{20}$$
$$B_{eq} = \frac{1}{r_W^2}\left(B_d + \frac{1}{K_g^2}B_m\right)$$

In order to obtain a complete integral causality, a greater effort in the initial stage is required but this feature allows us to obtain the control scheme systematically. We next present the procedure needed to find this control.

3. Inversion based control of the studied EV

The control scheme of the vehicle is deduced from an inversion of the EMR [12,13]. The tuning path presented in Fig. 3(a) is defined according to the objective and constraints of the system. It shows that the aim is to control the vehicle velocity using the signal input **S** of the chopper as the tuning variable. The control path is then deduced by inverting the tuning path (see Fig. 3(b)). Elements along the control path are inverted as follows: accumulation elements are inverted using a closed-loop control; distribution elements are inverted using criteria or compensation; conversion elements are inverted directly.

Next, the control equations within each control block are deduced based on the inversion of the EMR obtained in Section 2.3.

3.1. Inversion of the chassis

In order to invert the longitudinal dynamics, a controller is required to yield the reference F^*_{tot} using the measured and reference velocities (V_x and V^*_x, respectively). F_{env} can also be used as compensation as follows:

$$F^*_{tot} = C_{s1}(t)\left[V^*_x - V_x\right] + F_{env} \tag{21}$$

where $C_{s1}(t)$ may be any controller. In our application, a PI-Controller is used with parameters K_{P1} and K_{I1} which correspond to the proportional and integral gains, respectively.

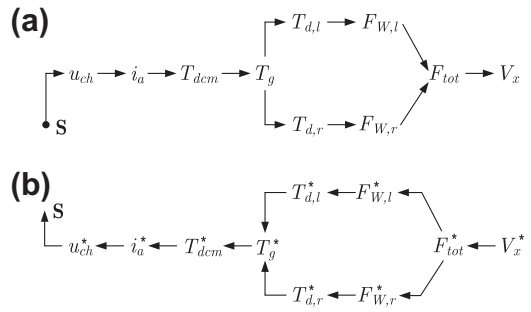

Fig. 3. (a) Tuning paths of the electric vehicle and (b) control paths.

After obtaining F^*_{tot}, the inversion of the mechanical coupling needs a supplementary input (k_1) in order to determine the contribution of each wheel to the total force:

$$F^*_{W,l} = k_1\, F^*_{tot}$$
$$F^*_{W,r} = (1 - k_1)\, F^*_{tot} \tag{22}$$

3.2. Inversion of the wheels and mechanical differential

The reference torque applied to each wheel $\left(T^*_{d,i}\right)$ can be obtained by inverting (18) as follows:

$$T^*_{d,i} = r_W F^*_{W,i} \rightarrow i \in \{l, r\} \tag{23}$$

These reference torques are used to invert the mechanical differential from (17) in order to obtain the shaft torque (T_g). The contribution of each torque is again determined by a supplementary input (k_2) given by the control strategy, as shown:

$$T^*_g = k_2\, T^*_{d,l} + (1 - k_2)\, T^*_{d,r} \tag{24}$$

3.3. Inversion of the gearbox

The fixed ratio of the gearbox given in (16) allows us to obtain the reference torque for the DC machine, as shown:

$$T^*_{dcm} = \frac{T^*_g}{K_g} \tag{25}$$

3.4. Inversion of the DC machine

By analyzing the dynamics of the machine given in (3) it is possible to determine the reference for the armature current. This is given as:

$$i^*_a = \frac{T^*_{dcm}}{K_{dcm}} \tag{26}$$

Another controller is required to set the reference voltage for the chopper u^*_{ch}. This controller requires the measured (i_a) and reference (i^*_a) armature currents. The electromotive force (e_a) can also be used as compensation, as can be seen from:

$$u^*_{ch} = C_{s2}(t)\left[i^*_a - i_a\right] + e_a \tag{27}$$

where $C_{s2}(t)$ is the controller for the armature current. In our application a PI-Controller is used with parameters K_{P2} and K_{I2} which correspond to the proportional and integral gains, respectively.

3.5. Modulation strategy for the chopper

In order to determine the signal input **S**, a simple modulation strategy is used which applies $\pm u_{BAT}$ to the DC machine depending on u^*_{ch}, as follows:

$$S_{11} = sign(u^*_{ch} - g)$$
$$S_{12} = \overline{S}_{11}; \quad S_{21} = \overline{S}_{11}; \quad S_{22} = S_{11} \tag{28}$$

where the function g is a carrier high frequency triangular signal varying between u_{BAT} and $-u_{BAT}$ [29]. Using this technique, the first expression of (28) gives the duty cycle of the voltage applied to the DC machine.

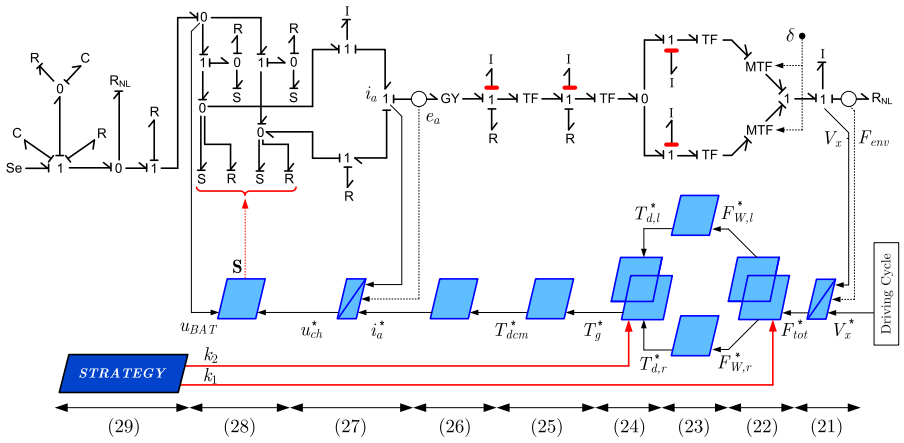

Fig. 4. EMR-based control applied to the Bond Graph representation of the EV.

3.6. Global strategy

The final step is to determine the overall control strategy [30,31]. In our application, it is defined by setting the values of k_1 and k_2.

The first supplementary input needed in (22) is used to split the contribution of each wheel to the total force. This strategy is used to optimize the transmitted torque when a wheel is skidding in order to stabilize the vehicle [32]. Given that in our application both wheels are assumed identical, the same contribution is required for each wheel.

The second supplementary input needed in (24) is used to invert the differential. Given the mechanical constraint, both supplementary inputs must be equal. For this study they are fixed as follows:

$$\begin{aligned} k_1 &= 0.5 \\ k_2 &= 0.5 \end{aligned} \tag{29}$$

All the equations concerning the developed control strategy are summarized in (21)–(29). The global scheme of the EMR-based control is finally depicted in Fig. 4.

4. Simulation results

Simulation results are obtained from the model of Fig. 4 which is implemented using 20SIM® [33]. This software includes a BG library and solvers for derivative relationships. Also, a specific EMR library has been developed, making the simulation environment ideal for this application. Details about the implementation in 20SIM® are given in Appendix B.

The numerical experiment proposed in this Section aims to analyze the performance of the proposed control scheme along two Urban Driving Cycles (UDC), as shown in Fig. 5(a). Additionally, two turning maneuvers are performed during the first UDC. First the vehicle turns left and then it turns right. Fig. 5(b) shows the angular velocity of the wheels. It can be seen that, during the turning maneuver, the angular velocity of the wheels are different, while the vehicle velocity remains equal to the reference velocity.

According to the control scheme, a second controller is also necessary to settle the armature current which defines the torque of the DC machine. A slope is also simulated during the second UDC. Fig. 5(c) shows the demanded current. It is proved that the controller is able to compensate the additional torque required which is reflected in the armature current.

The presented model allows us to evaluate the global energy performance. Fig. 6(a) shows the state of charge and Fig. 6(b) shows the total energy delivered by the batteries during the UDCs. It can be seen that during the braking maneuver, the battery is charged due to the regenerative braking.

Simulation results validate the proposed control scheme and illustrate the multi-domain feature of the model. Table 1 depicts the parameters of the complete system.

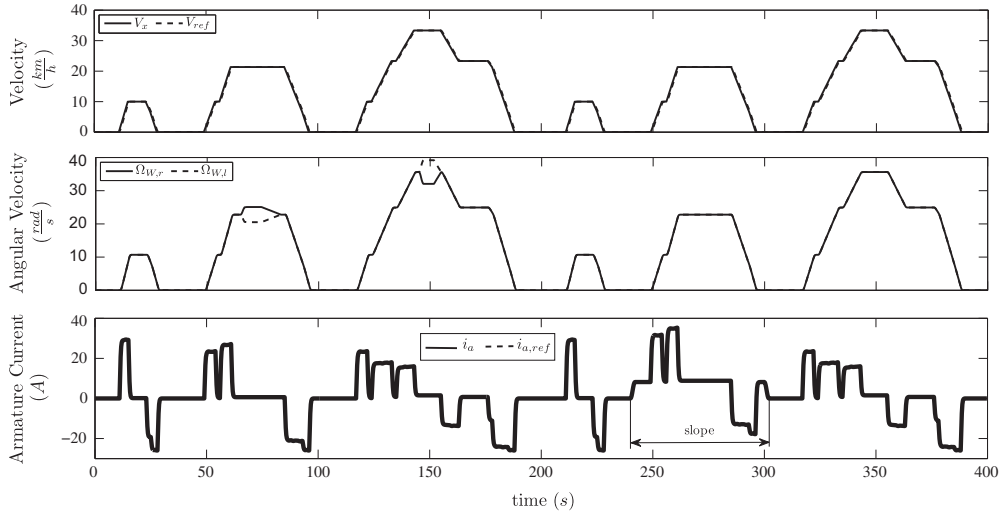

Fig. 5. (a) Vehicle velocity, (b) angular velocities of the wheels, and (c) armature current during the UDC.

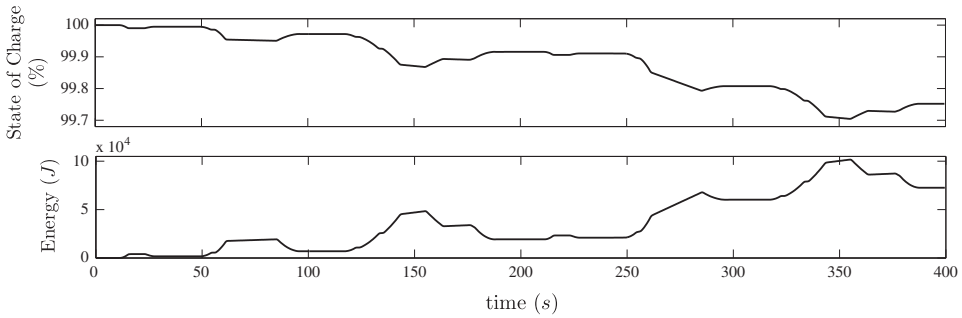

Fig. 6. (a) State of charge and (b) energy delivered by the battery.

Table 1
Complete system parameters.

Battery			
C_0	1835 (A h)	K_c	1.18
θ	313 (°K)	θ_f	233 (°K)
ϵ	1.29	δ	1.4
I^*	50 (A)	K_e	580×10^{-6}
E_{m0}	300 (V)	τ_1	5000 (s)
R_{00}	2×10^{-3} (Ω)	R_{10}	0.7×10^{-3} (Ω)
R_{20}	15×10^{-3} (Ω)	A_0	−0.3
A_{21}	−8	A_{22}	−8.45
u_{p0}	0.1 (V)	A_p	2
G_{p0}	2×10^{-12} (S)		
Chopper			
R_{on}	10×10^{-3} (Ω)	R_{off}	1×10^{6} (Ω)
DC machine			
R_{eq}	0.35 (Ω)	L_{eq}	6.5×10^{-3} (H)
K_{dcm}	1.24 (Nm/A)		
Shafts/gearbox			
J_m	0.12 (kg m^2)	B_m	1.08×10^{-3} (Nm s)
K_g	5		
Differential/wheels			
J_d	3.65 (kg m^2)	B_d	0.015 (Nm s)
J_W	4.3 (kg m^2)	r_W	0.26 (m)
Chassis			
d	1.1 (m)	l	1.7 (m)
M_{veh}	960 (kg)		
Environment			
ρ_{air}	1.223 (kg/m^3)	A_f	1.4 (m^2)
C_x	0.35	K_r	1.2×10^{-3}
g	9.81 (m/s^2)	φ	0°
Control			
K_{P1}	9540 (Ns/m)	K_{I1}	2.5 (N/m)
K_{P2}	10.15 (Ω)	K_{I2}	417.8 (Ω/s)

5. Conclusion

This research addresses the simulation of an electric vehicle, including the controllers. In order to highlight the energy distribution, the model of the physical system is represented using Bond Graph (BG), the structural approach, which provides a direct correspondence with the real physical system. This feature allows us to intuitively include faults. The control scheme is deduced systematically from the Energetic Macroscopic Representation (EMR), the functional approach, of the vehicle. In order to couple the representation of the vehicle and its control, a specific EMR library has been developed in the 20SIM® software, which is dedicated mostly to BG models.

Our contribution allows us to exploit the particular advantages of both approaches and allows any EMR/BG representation to be generated in 20SIM®. The proposed combination of structural and functional approaches used to study the complete system behavior is a useful simulation tool because it can be extended to any complex and large scale physical system.

Further research will use this coupling proposal to study different fault operations.

Appendix A. Details of both modeling approaches

The commonly used elements and their behavior are presented in Table 2.

Table 2
Synoptic of elements.

Bond Graphs			
Source of effort Se	$e = E$ $f \rightarrow$ fixed by the system	**Source of flow** Sf	$f = F$ $e \rightarrow$ fixed by the system
Capacitor C	$e(t) = \frac{1}{C}\int_{t_0}^{t} f(\tau)d\tau + e(t_0)$	**Inertia** I	$f(t) = \frac{1}{I}\int_{t_0}^{t} e(\tau)d\tau + f(t_0)$
Resistor R	$e - Rf = 0$	**Switch** S	$f = s\frac{1}{R_{on}}e$ $s \rightarrow$ boolean variable
1-Junction 1	$f_1 = f_2 = \ldots = f_n$ $\sum_{j=1}^{n} \pm e_j = 0$	**0-Junction** 0	$e_1 = e_2 = \ldots = e_n$ $\sum_{j=1}^{n} \pm f_j = 0$
Transformer TF	$e_2 - K e_1 = 0$ $f_1 - K f_2 = 0$	**Gyrator** GY	$f_2 - K e_1 = 0$ $f_1 - K e_2 = 0$

Energetic Macroscopic Representation	
Source of Energy generator and/or receptor	**Multiphysical Converter** no energy accumulation
Control Block without controller inverted directly	**Monophysical Converter** without tuning variable no energy accumulation
Control Block with controller	**Accumulator Element** with energy accumulation
Control Block with coupling criterion	**Distribution Element** distribution of energy
Strategy Block determines the coupling criterion	**Monophysical Converter** with tuning variable no energy accumulation

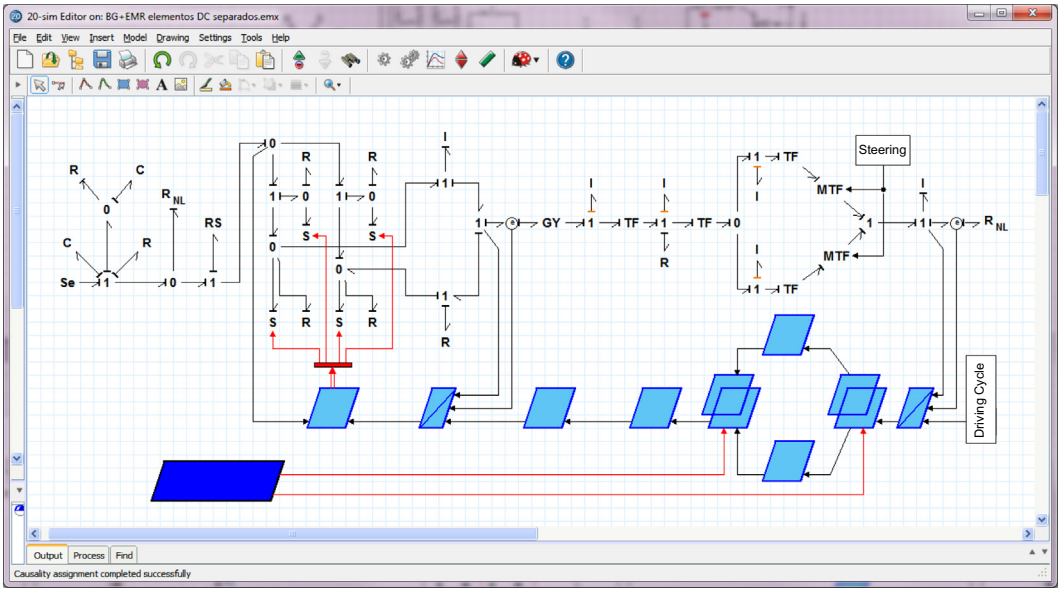

Fig. 7. Implementation of the model in the 20SIM® simulation environment.

Appendix B. Model implementation in 20SIM®

In order to implement the closed-loop system proposed in Fig. 4, it is necessary to generate a simulation environment where both approaches can coexist. To this end, the 20SIM® software is used, which is dedicated mostly to Bond Graph models. A specific EMR library was developed to couple both methods. In this library the topology of each block is identical to its equivalent representation in the EMR theory, thus making it possible to generate in 20SIM® an EMR/BG representation that coincides with its graphical representation.

The 20SIM® model of the vehicle in BG and its EMR-based control is depicted in Fig. 7. This model was used to obtain the simulation results.

References

[1] Chan C. The state of the art of electric, hybrid, and fuel cell vehicles. Proc IEEE 2007;95(4):704–18.
[2] Gao D, Mi C, Emadi A. Modeling and simulation of electric and hybrid vehicles. Proc IEEE 2007;95(4):729–45.
[3] Chan C, Bouscayrol A, Chen K. Electric, hybrid, and fuel-cell vehicles: architectures and modeling. IEEE Trans Veh Technol 2010;59(2):589–98.
[4] Onoda S, Emadi A. PSIM-based modeling of automotive power systems: conventional, electric, and hybrid electric vehicles. IEEE Trans Veh Technol 2004;53(2):390–400.
[5] Paynter HM. Analysis and design of engineering systems. Cambridge (MA): MIT Press; 1961.
[6] Gawthrop P, Bevan G. Bond-graph modeling. IEEE Control Syst Mag 2007; 27(2):24–45.
[7] Silva LI, de la Barrera PM, De Angelo CH, Aguilera F, Garcia GO. Multi-domain model for electric traction drives using bond graphs. J Power Electron 2011;11(4):439–48.
[8] Filippa M, Mi C, Shen J, Stevenson R. Modeling of a hybrid electric vehicle powertrain test cell using bond graphs. IEEE Trans Veh Technol 2005;54(3): 837–45.
[9] Rizzoni G, Guzzella L, Bauaman BM. Unified modeling of hybrid electric vehicle drivetrains. IEEE Trans Mechatron 1999;4(3):246–57.
[10] Trigui R, Badin F, Jeanneret B, Harel F, Coquery G, Lallemand R, et al. Hybrid light duty vehicles evaluation program. Int J Automot Technol 2003;4(2): 65–75.
[11] Wipke K, Cuddy M, Burch S. ADVISOR 2.1: a user-friendly advanced powertrain simulation using a combined backward/forward approach. IEEE Trans Veh Technol 1999;48(6):1751–61.
[12] Bouscayrol A, Pietrzak-David M, Delarue P, Pena-Eguiluz R, Vidal PE, Kestelyn X. Weighted control of traction drives with parallel-connected AC machines. IEEE Trans Ind Electron 2006;53(6):1799–806.
[13] EMR website: <http://emr.univ-lille1.fr/>.
[14] Murgovski N, Johannesson L, Sjoberg J. Engine on/off control for dimensioning hybrid electric powertrains via convex optimization. IEEE Trans Veh Technol 2013;62(7):2949–62.
[15] Wu FK, Yeh TJ, Huang CF. Motor control and torque coordination of an electric vehicle actuated by two in-wheel motors. Mechatronics 2013;23(1):46–60.
[16] Touati Y, Merzouki R, Bouamama BO. Robust diagnosis to measurement uncertainties using bond graph approach: application to intelligent autonomous vehicle. Mechatronics 2012;22(8):1148–60.
[17] Arogeti S, Wang D, Low CB, Yu M. Fault detection isolation and estimation in a vehicle steering system. IEEE Trans Ind Electron 2012;59(12):4810–20.
[18] Delarue P, Bouscayrol A, Barrade P. Energetic macroscopic representation and PSIM® simulation: application to a DC/DC converter input filter stability. In: 2010 IEEE vehicle power and propulsion conference (VPPC); 2010. p. 1–6.
[19] Einhorn M, Conte FV, Kral C, Fleig J. Comparison, selection, and parameterization of electrical battery models for automotive applications. IEEE Trans Power Electron 2013;28(3):1429–37.
[20] Merzouki R, Ould-Bouamama B, Djeziri M, Bouteldja M. Modelling and estimation of tire-road longitudinal impact efforts using bond graph approach. Mechatronics 2007;17(2–3):93–108.
[21] Sampaio R, Becker M, Lemos V, Siqueira A, Ribeiro J, Caurin G. Robust control in 4×4 hybrid-converted touring vehicles during urban speed steering maneuvers. In: 2010 IEEE vehicle power and propulsion conference (VPPC); 2010. p. 1–6.
[22] Barsali S, Ceraolo M. Dynamical models of lead–acid batteries: implementation issues. IEEE Trans Energy Convers 2002;17(1):16–23.
[23] Buller S, Thele M, De Doncker R, Karden E. Impedance-based simulation models of supercapacitors and li-ion batteries for power electronic applications. IEEE Trans Ind Appl 2005;41(3):742–7.
[24] Silva LI, De Angelo CH. Bond graph-based models of lead–acid batteries. Application to electric vehicles. In: 8th Symposium on power plant and power systems control; 2012. p. 1–6.
[25] Gonzalez-Contreras B, Rullan-Lara J, Vela-Valdes L, Claudio SA. Modelling, simulation and fault diagnosis of the three-phase inverter using bond graph. In: IEEE international symposium on industrial electronics, ISIE 2007; 2007. p. 130–5.
[26] Dauphin-Tanguy G, Rombaut C. Why a unique causality in the elementary commutation cell bond graph model of a power electronics converter. In: International conference on systems, man and cybernetics, 1993. 'Systems engineering in the service of humans', conference proceedings, vol. 1; 1993. p. 257–63.
[27] Karnopp DC, Margolis DL, Rosenberg RC. System dynamics: modeling and simulation of mechatronic systems. New York (USA): Willey InterCiences; 2000.
[28] Chen K, Bouscayrol A, Berthon A, Delarue P, Hissel D, Trigui R. Global modeling of different vehicles. IEEE Veh Technol Mag 2009;4(2):80–9.
[29] Holtz J. Pulse width modulation for electronic power converters. In: Bimal Bose K, editor. Power electronics and variable frequency drives. New York: IEEE Press; 1997.
[30] Johannesson L, Asbogard M, Egardt B. Assessing the potential of predictive control for hybrid vehicle powertrains using stochastic dynamic programming. IEEE Trans Intell Transport Syst 2007;8(1):71–83.
[31] Murgovski N, Johannesson L, Sjoberg J, Egardt B. Component sizing of a plug-in hybrid electric powertrain via convex optimization. Mechatronics 2012;22(1):106–20.
[32] Wang J, Wang Q, Jin L, Song C. Independent wheel torque control of 4WD electric vehicle for differential drive assisted steering. Mechatronics 2011;21(1):63–76.
[33] 20SIM website: <http://www.20sim.com/>.